Acta Crystallographica Section D
Biological Crystallography
ISSN 0907-4449

Refined structure of orthorhombic lysozyme crystallized at high temperature: correlation between morphology and intermolecular contacts

Hideyuki Oki,[a]† Yoshiki Matsuura,[a]* Hiroshi Komatsu[b] and Alexander A. Chernov[c,d]

[a]Institute for Protein Research, Osaka University, Suita, Osaka 565, Japan, [b]Institute for Materials Research, Tohoku University, Katahira, Aoba-ku, Sendai 980-77, Japan, [c]Universities Space Research Association, 4950 Corporate Drive, Suite 100, Huntsville, AL 35805, USA, and [d]Institute of Crystallography, Academy of Sciences, Leninskii Prospekt, Moscow 117333, Russian Federation

† Present address: Takeda Chemical Ind. Ltd, Juso-honmachi, Yodogawa-ku, Osaka, Japan.

Correspondence e-mail: matsuura@protein.osaka-u.ac.jp

Received 26 March 1998
Accepted 24 June 1998

PDB Reference: orthorhombic lysozyme, 1bg1.

The structure of orthorhombic hen egg-white lysozyme (HEWL) crystallized at 310 K has been refined at 1.7 Å resolution. Large displacements of the side-chain atoms with respect to the tetragonal structure were observed in many places, in contrast to small displacements of the main-chain atoms. A chloride-ion binding site was observed at an interface of two molecules, but at a different position to the binding site in the tetragonal form. The analysis of intermolecular contacts in the crystal has shown the presence of three independent intermolecular contacts which are called macrobonds *A*, *B* and *C*. Arginine side chains are frequently involved in these macrobonds, suggesting that the high frequency of this residue in HEWL may be a possible reason for the multiple polymorphs of this protein. The crystal forms were determined using a light-reflecting device on a four-circle diffractometer. Correlations between crystal forms and the three-dimensional macrobond networks were interpreted in terms of their components in various crystallographic planes, making use of approximate strengths of hydrogen-bond and van der Waals interatomic forces.

1. Introduction

Hen egg-white lysozyme has been extensively studied as a model of protein-crystal growth. It is also known to form various polymorphic crystals depending upon additive ions, pH and temperature. At least four crystal forms are known: tetragonal, orthorhombic, monoclinic and triclinic (Steinrauf, 1959), and these crystal structures have been determined (Blake *et al.*, 1962; Berthou *et al.*, 1983; Hodsdon *et al.*, 1990; Rao & Sundaralingam, 1996; Harata, 1994; Madhusudan *et al.*, 1993). Such a multiply polymorphic character is not often reported for a protein molecule, though it may be a general phenomenon arising from small differences in the potential energies of molecular contacts among various polymorphs. To understand this important phenomenon, we are studying the intermolecular contacts in these crystals and comparing the modes of atomic interactions among them, using HEWL as a starting model. Our aim is also to understand the role of these various intermolecular interactions in protein-crystal growth. During the search of the refined structures of the polymorphic HEWL crystals, we noticed that the structure entry for the orthorhombic crystal (2LZH) in the Protein Data Bank (Bernstein *et al.*, 1977) does not contain fully refined atomic coordinates. For completeness of the crystal structures of every crystal form, we have determined the high-temperature (310 K) crystallized form of orthorhombic HEWL and refined the structure at 1.7 Å resolution. Here, we describe the

structure of this crystal and compare the types of intermolecular interaction with those in the other crystal structures, especially the tetragonal form which has recently been refined at high resolution (Vaney *et al.*, 1996).

2. Materials and methods

2.1. Crystallization and structure determination

Crystallization was performed by the batch method in a water bath maintained at 310 K. The solution for crystallization was prepared in the same way as described by Jollès & Berthou (1972). Briefly, 500 mg of commercially available HEWL (crystallized six times; Seikagaku Kogyo Co.) was dissolved in 5 ml of water in a capped glass vial. To this solution, 0.625 ml of 0.2 *M* acetate buffer pH 4.7 and 1.875 ml water were added, followed by addition of 7.5 ml of a 100 mg ml^{-1} NaCl solution. The prepared solution was transferred to the water bath for 2 d in order to obtain crystals of sufficient size for X-ray diffraction experiments. The crystals typically grew to a size of 0.5 × 0.5 × 1 mm. A crystal was mounted and sealed in a thin-walled glass capillary for X-ray experiments with a small amount of crystallization mother liquor. The space group was $P2_12_12_1$ and the unit-cell dimensions were determined to be a = 56.44, b = 73.73 and c = 30.43 Å, with four molecules in the unit cell and a solvent content of 44% by volume. Intensity data collections were performed at 283 K using a Rigaku AFC-5R four-circle diffractometer with Ni-filtered monochromated Cu $K\alpha$ radiation (λ = 1.5418 Å) from a rotating-anode X-ray generator operated at 40 kV and 300 mA. The intensities of three standard reflections were monitored every 100 reflections to check crystal orientation and radiation damage. After collection of all data at 1.7 Å resolution, the final average decrease in the intensities of the monitoring reflections arising from radiation damage was 8%. The absorption effects were measured by azimuthal scanning of the (006) reflection about the φ-axis. The intensities of all other reflections were corrected for the effects of absorption according to the empirical method of North & Phillips (1968) and for radiation damage effects using the intensity changes of the monitor reflections. A total of 11 992 independent reflections [$F > \sigma(F)$] was collected. The initial structure was determined by the molecular-replacement method with the program *AUTOMR* (Matsuura, 1991) using the triclinic lysozyme molecule (PDB code 2LZT) as a search model. This process unambiguously gave the correct initial model of the crystal structure of orthorhombic lysozyme with an R factor of 0.39 and correlation coefficient of 0.72 at 2 Å resolution. This starting model was further submitted to simulated-annealing refinement using the program *X-PLOR* (Brünger *et al.*, 1987) at 1.7 Å resolution. The final results of the refinement including 1002 protein atoms, 109 water molecules and one chloride ion gave an R factor of 0.186. A summary of the refinement statistics is given in Table 1. The atomic coordinates and structure factors have been deposited in the Protein Data Bank (Bernstein *et al.*, 1977).

2.2. Observation of crystal-growth habit

In order to determine the Miller indices of the developed faces of a crystal, we devised a simple attachment for mounting onto the four-circle diffractometer. The construction of the instrument is shown in Fig. 1. The light-emitting diode and the microscope (60× magnification) were installed in the equatorial diffraction plane in an equi-angle from the χ-circle plane, so that the crystal face of a Miller plane in a diffracting geometry could also reflect the light that is observed by the microscope. An orthorhombic lysozyme crystal in a sealed glass capillary was mounted on the four-circle diffractometer, and the orientation matrix was determined by the X-ray diffraction method. The four-circle angles of a Miller plane with the lowest indices for the three crystal axes were then calculated, and the crystal was oriented at these angles, observing the reflected light from the crystal face. The Miller indices of the developed crystal faces are determined by repeating this process for other crystallographic planes.

3. Results

3.1. Overall crystal structure

The overall structure of the molecule is essentially the same as that of tetragonal lysozyme, with the root-mean-square deviations of all atoms and backbone atoms being 1.2 and 0.48 Å, respectively. The largest deviation among the backbone atoms was seen at the loop residues flanking the active cleft, Pro70, Gly71, Ser72 and Arg73, with the mean deviation being 1.4 Å. The second largest deviation occurs at Gly102 with a value of 1.0 Å. The deviations of the catalytic residues Glu35 and Asp52 were small (about 0.1 Å). The Debye–Waller factors of the backbone atoms showed a variation along the amino-acid sequence similar to that of tetragonal lysozyme. We also collected intensity data at the temperature of crystallization (310 K), expecting some structural changes compared with 283 K arising from a different modification at high temperature; however, the structures turn out to be

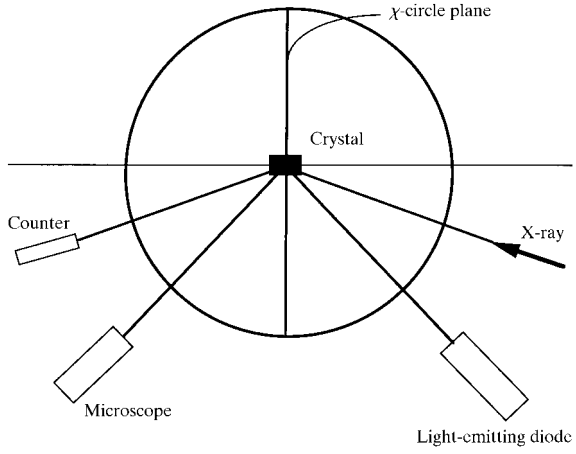

Figure 1
Construction of the device for observing the reflected light from a crystal face mounted on a four-circle diffractometer.

Table 1
Summary of refinement statistics.

R factor	0.186
R_{free} value	0.216
Standard deviations	
Bond length (Å)	0.007
Bond angle (°)	1.436
Dihedral angle (°)	22.2
Average temperature factors (Å^2)	
Main-chain atoms	15.0
Side-chain atoms	17.6
Water molecules	39.7
Chloride ion	20.0

almost identical and the final average temperature factors for all amino-acid atoms for the low- and high-temperature data were 17.0 and 17.4 Å^2, respectively. Since the structures, as well as the temperature factors, are almost the same, we shall describe the structure of the orthorhombic lysozyme based on the 283 K structure.

3.2. Side-chain structure

In the present crystal structure, the reported alternative conformations in tetragonal lysozyme at Lys1, Ser86 and Val109 (Vaney *et al.*, 1996) were found only at the Ser86 side chain. The occupancy factors of the two alternative Ser86 O$^\gamma$ sites were refined, resulting in occupancy factors of 0.7 and 0.3 for the major and minor sites, respectively. In either conformation, the O$^\gamma$ atom is hydrogen bonded to two bound water molecules which stabilize the conformation. The positions of the O$^\gamma$ atoms are similar to those found in the tetragonal form. Large displacements of side-chain atoms with respect to the tetragonal molecule were observed in residues Phe3, Glu7, Lys13, Arg14, Asn19, Arg21, Phe34, Arg45, Asn46, Tyr53, Arg61, Arg68, Arg73, Lys97, Asp101, Asn103, Asn106, Val109, Lys116, Asp119, Arg125 and Leu129, in all of which at least one atom is observed to deviate by more than 2 Å.

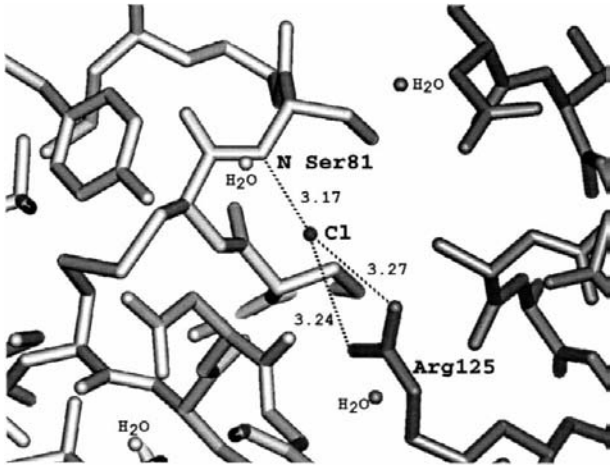

Figure 2
Environments of the chloride ion which is bound at the interface of two molecules (macrobond *A*). The dark and light skeletons show different molecules.

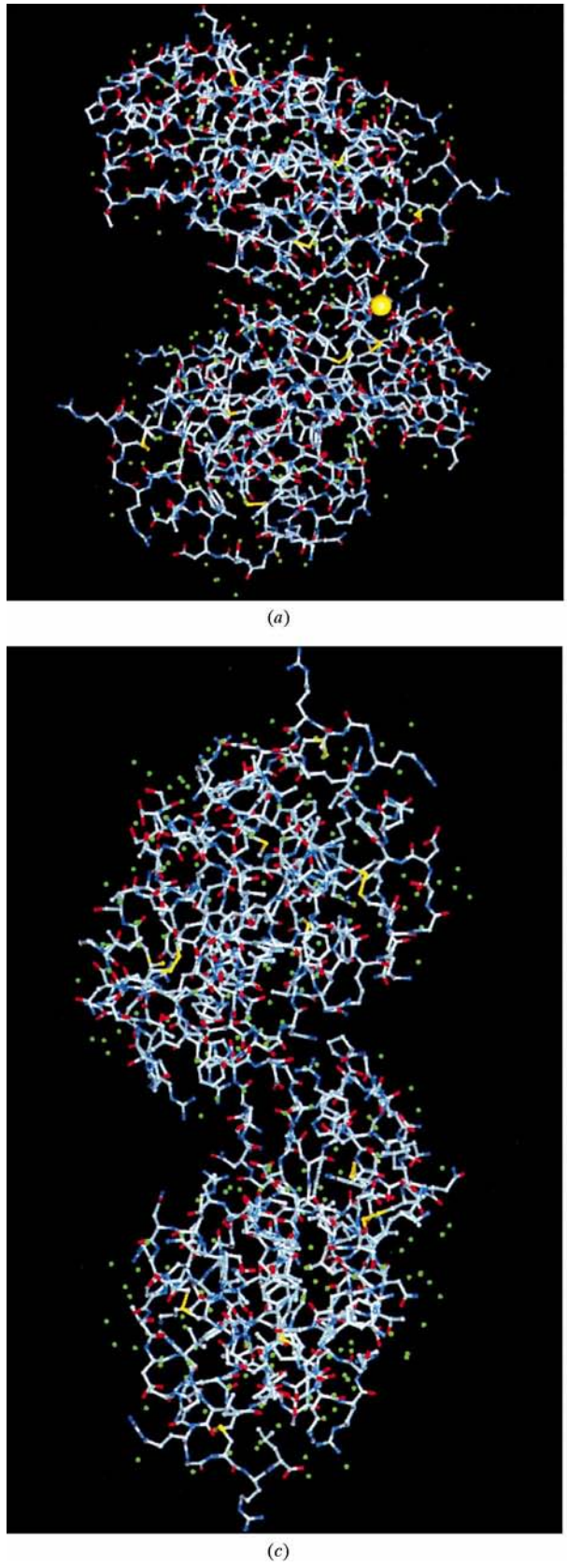

Figure 3
Appearances of the contacts of the two molecules *via* (*a*) macrobond *A*, (*b*) macrobond *B* and (*c*) macrobond *C*. A yellow sphere in (*a*) shows the bound chloride ion.

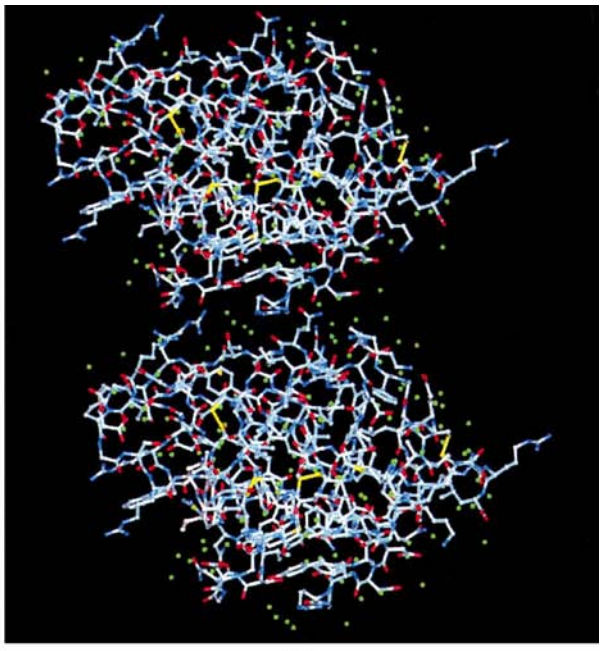

Figure 3 (continued)

3.3. Anion binding

The stereochemical environment around the chloride ion is shown in Fig. 2. This chloride ion was found to be hydrogen bonded or to form a salt bridge to the side-chain imino group of Arg125 with an average $N^{\eta}\cdots Cl$ distance of 3.25 Å, as shown in Fig. 2. On the other hand, this ion is also involved in intermolecular binding, being hydrogen bonded to the main-chain N atom of Ser81 of a symmetry-related molecule with the Cl$\cdots$N distance being 3.17 Å. In tetragonal lysozyme, a chloride ion is also bound at an interface of two molecules, but the residues involved in the chloride ion binding are different. The counter-ion of the chloride, a sodium ion which has been reported as being bound near Ser72 O^{γ} in the tetragonal form (Vaney *et al.*, 1996), is not clearly identified in the present structure, although two water molecules with reasonable Debye–Waller factors (both 20 $Å^2$) seem to make hydrogen bonds to the chloride ion. The temperature factor of Ser72 O^{γ} in the present structure is large (36.8 $Å^2$) with an electron-density distribution elongated toward one of the two water molecules, which was assigned as a sodium ion in the tetragonal crystal, suggesting a local disorder in this region. The backbone carbonyl O atom of Arg73, which is directed toward the putative position of the sodium ion in the tetragonal structure (Vaney *et al.*, 1996), is directed oppositely in the orthorhombic structure, thus making the octahedral coordination geometry incomplete.

3.4. Intermolecular contacts

In the present orthorhombic lysozyme crystal, each molecule is surrounded by six symmetry-related molecules – that is, a molecule in a general position at (x, y, z) has contacts with those in positions $(x-\frac{1}{2}, \frac{1}{2}-y, 1-z)$, $(x+\frac{1}{2}, \frac{1}{2}-y, 1-z)$, $(x, y, z-1)$, $(x, y, z+1)$, $(\frac{1}{2}-x, 1-y, z-\frac{1}{2})$ and $(\frac{1}{2}-x, 1-y, z+\frac{1}{2})$. Here, the molecules are designated to be contacting if they have at least one intermolecular atomic distance less than 4 Å, including cases where one of the atom pair is a bound water molecule. Of these contacting molecules, each pair of successive positions in the above listing are related by a simple translation of the repeating lattice unit, forming the same interatomic interactions within the pairs: the first pair is related by a lattice translation of one unit along the *a* axis, the second pair by two units along the *c* axis and the third pair by one unit along the *c* axis. As a result, only three independent intermolecular contacts exist in the crystal. We named these macrobonds *A*, *B* and *C* for the intermolecular interactions between (x, y, z) and $(x-\frac{1}{2}, \frac{1}{2}-y, 1-z)$, $(x, y, z-1)$ and $(\frac{1}{2}-x, 1-y, z-\frac{1}{2})$, respectively, as shown in Table 3. The pattern of the macrobonds could be visually recognized by plotting intermolecular-distance maps (Matsuura *et al.*, 1979) (data not shown). The overall appearance of the molecular contacts in each macrobond is shown in Fig. 3. The total numbers of non-hydrogen interatomic distances less than 4 Å are 108, 69 and 50, respectively, for macrobonds *A*, *B* and *C*. Of these, the numbers of direct hydrogen bonds between amino-acid residue atoms (including the chloride ion) are 6, 5 and 2, respectively. The numbers of bound water molecules involved in the intermolecular hydrogen bonds are 18, 10 and 9,

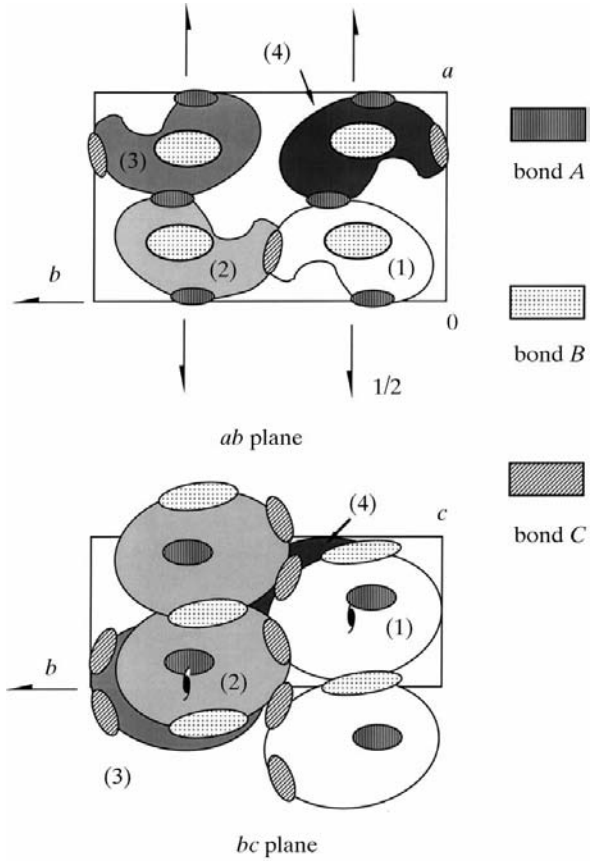

Figure 4
A schematic diagram of the molecular packing projected from the *c*-axis (upper) and *a*-axis (lower) directions. The locations of macrobonds are also shown.

Table 2
Summary of number of intermolecular atomic interactions in macrobonds.

Macrobond	*A*	*B*	*C*
Total number	108	69	50
Direct hydrogen bond	6	5	2
Water-mediated hydrogen bond	18	10	9
Other interactions†	84	54	39
Macrobond energy (kcal mol^{-1})	70.2	46.2	31.2

† Number of other atom pairs with distances less than 4 Å.

respectively. The numbers of intermolecular atomic pairs composed of neutral atoms with distances less than 4 Å are 84, 54 and 39, respectively, and these are assumed to be van der Waals interactions, since inspection of the whole list of atom pairs shows they are mostly composed of non-repulsive pairs. These results are summarized in Table 2 for the macrobonds *A*, *B* and *C*. The hydrogen-bonded amino-acid atom pairs involved in the three intermolecular contacts are listed in Table 3. As shown in Table 3, the chloride ion is involved in macrobond A with the stereochemical environment described in §3.3. Schematic diagrams of the molecular packing in the crystal lattice and the sites of macrobonds *A*, *B* and *C* are shown in Fig. 4.

3.5. Crystal morphology

The crystal-growth habit of the orthorhombic lysozyme is sketched in Fig. 5. Shown in this figure are the Miller indices of the developed faces, as determined by the method described in §2.2. The crystal has a tendency to elongate along the crystallographic *c* axis with development of the (110) and (1$\bar{1}$0) faces. The end of the rod is formed by the (011) and (0$\bar{1}$1) faces. The narrow (010) face is also seen along the *c* axis.

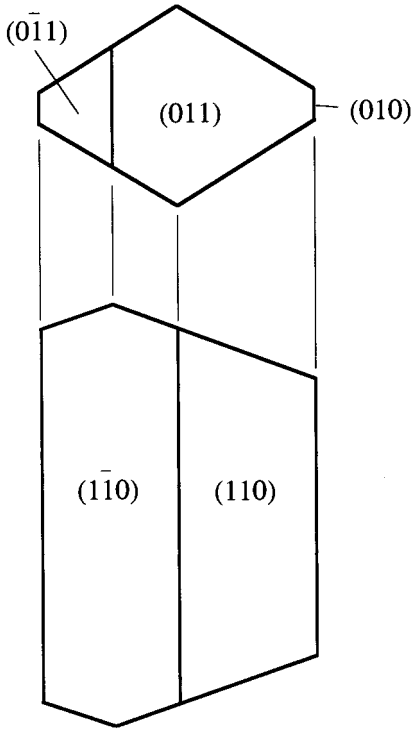

Figure 5
Illustration of the crystal-growth habit of the orthorhombic lysozyme with Miller indices of the crystal faces

Table 3
Direct hydrogen bonds between amino-acid residue atoms (including the chloride ion) involved in the intermolecular contacts.

Macrobond *A*

Molecule at (x, y, z)	Molecule at ($x-\frac{1}{2}$, $y+\frac{1}{2}$, $1-z$)	Distance (Å)
Asn113 O	Ser85 O$^{\gamma}$	3.14
Asp119 O	Ser81 O$^{\gamma}$	2.93
Arg125 N$^{\eta1}$	Asn65 O	3.12
Arg125 N$^{\eta2}$	Asp66 O	3.42
Arg125 N$^{\eta1}$	Cl	3.27
Arg125 N$^{\eta2}$	Cl	3.24

Macrobond *B*

Molecule at (x, y, z)	Molecule at (x, y, $z-1$)	Distance (Å)
Asn39 N$^{\delta2}$	Asn19 O	3.48
Gln41 O$^{\varepsilon1}$	Arg21 N	3.01
Gln41 O$^{\varepsilon1}$	Arg21 N$^{\eta1}$	2.63
Arg45 N$^{\varepsilon}$	Gly102 O	2.99
Arg45 N$^{\eta2}$	Val99 O	3.52

Macrobond *C*

Molecule at (x, y, z)	Molecule at ($\frac{1}{2}-x$, $1-y$, $z-\frac{1}{2}$)	Distance (Å)
Arg61 N$^{\eta1}$	Gly102 O	2.99
Arg61 N$^{\eta2}$	Gly102 O	2.64

4. Discussion

4.1. Possible origin of polymorphs

Polymorphism is well known for numerous protein and organic molecule crystals. HEWL is a typical example, since it crystallizes in at least four different crystal systems depending on the precipitants and temperature. There also are several studies reporting phase transitions with changes of temperature and humidity (Jollès & Berthou, 1972; Madhusudan *et al.*, 1993). These variabilities of the crystal structure are characteristic for this protein. As shown in Table 3, arginine side chains frequently occur in every intermolecular contact in the present crystal. We found that the same residues are also frequently involved in intermolecular contacts in other crystal forms, though their side-chain conformations vary from crystal to crystal (all data is not shown). A visual comparison of the arginine side-chain conformations in orthorhombic and tetragonal forms is given in Fig. 6. In these crystal forms, different arginine residues are involved in the intermolecular interactions. In HEWL, there are 11 arginine residues per 129 residues (8.5%), which is high compared with the average abundance of this residue of 3% in proteins (Singh &

Thornton, 1992). The hydrophilic residue arginine has a tendency to be exposed at the surface of the molecule, as shown in Fig. 6, which provides more chances for it to be involved in intermolecular interactions. Furthermore, this residue is flexible owing to the long side chain with a positively charged imino group at its end, allowing it to adopt various conformations and thus enable a variety of modes of interaction with other molecules. As a result, we infer that the presence of many arginine residues over the surface of the molecule might be one of the important reasons for the polymorphism of this protein. Recently, the frequent involvement of arginine residues in protein interfaces has also been shown from a survey of various protein crystals (Dasgupta *et al.*, 1997).

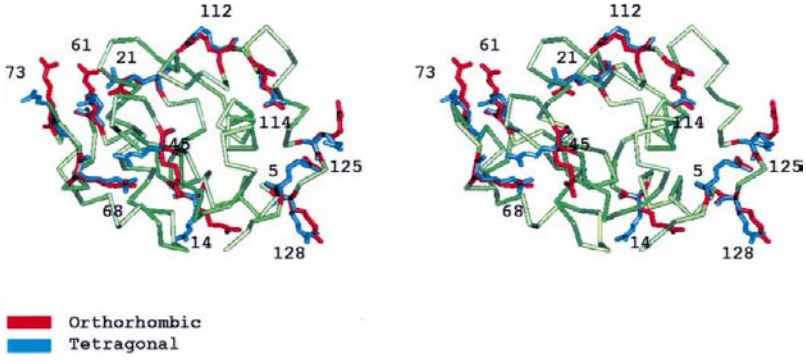

Figure 6
A stereoscopic view of a superposition of the orthorhombic and tetragonal lysozyme molecules focusing on the orientations of arginine side chains, shown in red and blue, respectively. The residue numbers of the arginines are indicated.

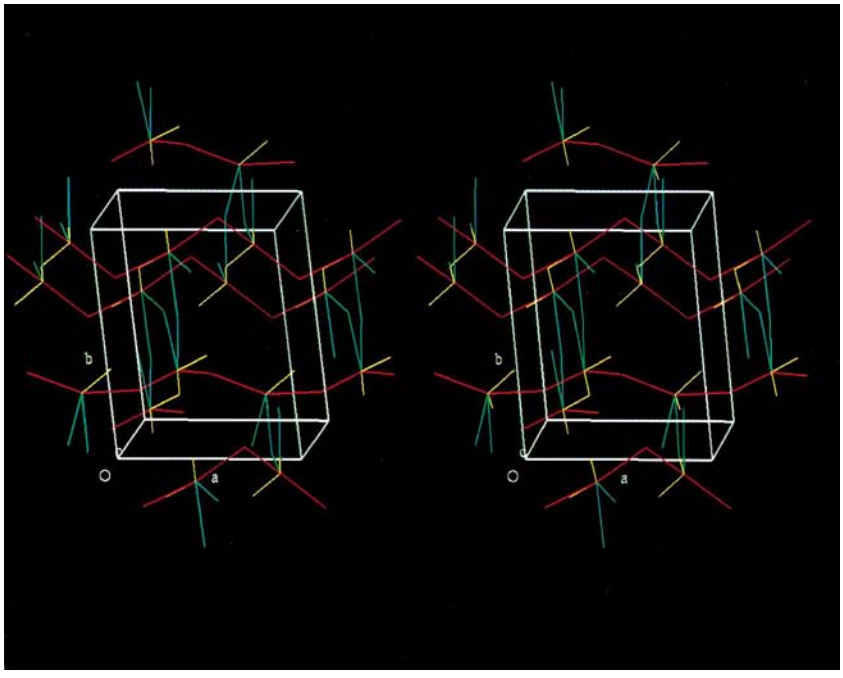

Figure 7
A stereoscopic view of macrobond chains in the orthorhombic crystal. The macrobonds *A*, *B* and *C* are shown as red, yellow and blue lines, respectively, connecting the contact site and the centre of molecules. $V^{\rm across}(hkl)$ was derived by studying this picture from various directions by rotation of the computer graphics.

4.2. Correlation of the macrobond energy and crystal habit

There have been several studies focused on molecular packing in protein crystals (Crosio *et al.*, 1990, 1992; Svensson *et al.*, 1991; Janin & Rodier, 1995; Dasgupta *et al.*, 1997), packing analysis studied using the periodic bond chain (PBC) theory of Hartman and Perdok (Hartman & Perdok, 1955*a*,*b*,*c*; Frey *et al.*, 1991; Nadarajah & Pusey, 1996) and computer simulations of crystal growth (Durbin & Feher, 1991; Strom & Bennema, 1997*a*,*b*). Our present study is also focused on the nature of the intermolecular interactions and morphology of orthorhombic lysozyme. The molecular packing and the locations of the three macrobonds in the present crystal structure are shown in Fig. 4. This figure gives only a qualitative view of the intermolecular contacts. In contrast, as shown in Fig. 7, when each macrobond is extracted from the structure as a line connecting the contact site and molecular centres of the contacting molecules, we can obtain chains of macrobonds with respect to various crystallographic planes. To make a qualitative judgement on crystal habit we used the PBC approach, and first derived $V^{\rm across}(hkl)$, the number of component macrobonds which cross the unit area of crystallographic planes, using computer-graphics analysis as shown in Fig. 7 which depicts a view from one direction. Counting of the macrobonds crossing a plane has been performed by careful study of these pictures from various directions. The results are shown in Table 4. The sum of $V^{\rm across}$ for the planes (100), (010) and (001), $2A + 4B + 4C$, is one half of the total inter-unit-cell macrobonds (there are two planes of each type bordering the unit cell), and the bond count within a unit-cell is $2A + C$ for a cluster of the nearest four molecules in the unit cell, with one macrobond *C* being counted twice for (010) and (001) by reason of passing both planes. On the other hand, detachment of the unit cell molecule by molecule requires energy corresponding to $V^{\rm total} = 4A + 4B + 4C$, considering four molecules in the unit cell on the same scale (halved cell) to the values shown in Table 4. The net macrobond component to detach a whole unit cell from a half-crystal, *i.e.* kink position, thus becomes $V^{\rm total} - (2A + C) = 2A + 4B + 3C$, which equals the net sum of $V^{\rm across}$ for the planes (100), (010) and (001), considering double counting for one macrobond *C* as mentioned above. As a measure of the energy of all the macrobonds running within a plane, $V^{\rm within}(hkl)$ is calculated by using the complementary relation $V^{\rm within}(hkl) = V^{\rm total} - V^{\rm across}(hkl)$, where the

Table 4
Macrobond components and their total energies across and within various crystallographic planes.

Actual magnitudes of V and E should be doubled for a whole six-faced unit cell.

(hkl)†	$d(hkl)$ (Å)	$V^{\rm across}$	$V^{\rm within}$	$E^{\rm across}$ (kcal mol^{-1})	$E^{\rm within}$ (kcal mol^{-1})
(100)	56.4	$2A$	$2A + 4B + 4C$	140.4	450.0
(010)	73.7	$2C$	$4A + 4B + 2C$	62.4	528.0
(001)	30.4	$4B + 2C$	$4A + 2C$	247.2	343.2
(011)	28.1	$4B + 2C$	$4A + 2C$	247.2	343.2
(101)	26.8	$2A + 4B + 2C$	$2A + 2C$	387.6	202.8
(110)	44.8	$2A$	$2A + 4B + 4C$	140.4	450.0

† Those of planes having negative indices are equivalent to those of all-positive-indexed planes.

terms 'across' and 'within' correspond to 'attach' and 'slice', respectively, in Bennema's notation (Bennema, 1995). The $V^{\rm within}$ values thus calculated are also shown in Table 4. $V^{\rm within}$ represents the step energy on the face under consideration averaged over all possible azimuthal orientations of this step.

In the present paper, we estimated the relative bond strength semiquantitatively, by limiting the interaction pairs to only the atom pairs with distances less than 4 Å. The interaction pairs were classified, as shown in Table 2, as two kinds of hydrogen bonds, and the remaining pairs as attractive van der Waals interactions. We assumed interaction energies for these three types of macrobonds as follows. The hydrogen-bond energy ranges from 0.5 to 3 kcal mol^{-1} (1 kcal = 4.184 kJ) depending on the distance and direction (Frey *et al.*, 1991). In the present structure, we obtained average Debye–Waller factors of 17.0 and 39.7 Å^2 for amino-acid-residue atoms and bound water molecules, respectively. These values are correlated with the positional order of the atoms, and may also correlate to the strength of the bonds, including hydrogen bonds. Thus, we assumed 3 kcal mol^{-1} per hydrogen bond between amino-acid residue atoms (Kabsch & Sander, 1983) and 1.5 kcal mol^{-1} for water-mediated hydrogen bonds. For the van der Waals interactions, which were found to range from 0.2 to 0.5 kcal mol^{-1} in the Lennard–Jones potential function for model compounds (Reid *et al.*, 1985), we assumed 0.3 kcal mol^{-1} per interaction pair. In the last row of Table 2, the bond energies calculated in this way for each macrobond are shown. By using these bond energy values, the energies $E(hkl)$ across and within crystallographic planes are calculated as shown in the last two columns of Table 4. The energy within a plane corresponds to the degree of face development of that plane. The observed developed faces (011)/(0$\bar{1}$1), (110)/(1$\bar{1}$0) and (010) have relatively high values, 343.2, 450.0 and 528.0 kcal mol^{-1}, respectively, compared to others with the exception of the value for the (100) plane. The developed (011) and (110) and the undeveloped (001) and (100) faces have the same magnitude of values with the same macrobond components, as shown in Table 4. These facts and the phenomenon of unobserved faces with high energy values may be attributed experimentally to crystallization conditions, or using protein preparations of improved purity, and to the approximations associated with the PBC approach. Another factor may be the inaccuracy of E estimates which have been calculated using only limited atomic interaction pairs and also ignoring the effects of disordered solvent molecules which may greatly affect the surface properties of protein molecules. Recently, an AFM study of an orthorhombic HEWL crystal which possesses an extensively developed (010) face has been performed (Rashkovich *et al.*, 1998) observing two molecules on the surface of (010) plane, which is consistent with our results as indicated in Table 4 and Fig. 7. The correlation between $E^{\rm within}(hkl)$ and the interplanar spacing $d(hkl)$ of various planes is maintained (Table 4), as the Bravais–Friedel–Donnay–Harker law (Hartman, 1973) predicts, suggesting the estimation of the macrobond energies is essentially correct. The present analysis does not fully quantitatively account for the relation between macrobond energies and morphology of the orthorhombic HEWL crystal. However, it at least gives qualitative insights even under rough estimation of bond strengths. The present analysis has also shown that the development of faces may not be dictated only by macrobond energies but also by other factors, such as impurities and solvent effects.

The authors thank Dr S. Durbin for reading the manuscript and for useful discussions.

References

Bennema, P. (1995). *Science and Technology of Crystal Growth*, edited by J. P. van der Eerden & O. S. L. Bruinsma, pp. 149. Dordrecht: Kluwer Academic Publishers.

Bernstein, F. C., Koetzle, T. F., Williams, G. J. B., Meyer, E. F., Brice, M. D., Rodgers, J. R., Kennard, O., Shimanouchi, T. & Tasumi, M. (1977). *J. Mol. Biol.* **112**, 535–542.

Berthou, J., Lifchitz, A., Artymiuk, P. & Jollès, P. (1983). *Proc. R. Soc. London Ser. B*, **217**, 471–489.

Blake, C. C. F., Fenn, R. H., North, A. C. T., Phillips, D. C. & Poljak, R. J. (1962). *Nature (London)*, **196**, 1173–1176.

Brünger, A. T., Kuriyan, J. & Karplus, M. (1987). *Science*, **235**, 458–460.

Crosio, M.-P., Janin, J. & Jullien, M. (1992). *J. Mol. Biol.* **228**, 243–251.

Crosio, M.-P., Rodier, F. & Jullien, M. (1990). *FEBS Lett.* **271**, 152–156.

Dasgupta, S., Iyer, G. H., Bryan, S. H., Lawrence, C. E. & Bell, J. A. (1997). *Proteins*, **28**, 494–514.

Durbin, S. D. & Feher, G. (1991). *J. Cryst. Growth*, **110**, 41–51.

Frey, M., Taverne, J.-C. G. & Fontecilla-Camps, J. C. (1991). *J. Phys. D*, **24**, 105–110.

Harata, K. (1994). *Acta Cryst.* D**50**, 250–257.

Hartman, P. (1973). *Crystal Growth: An Introduction*, pp. 367. Amsterdam: North-Holland.

Hartman, P. & Perdok, W. G. (1955*a*). *Acta Cryst.* **8**, 49–52.

Hartman, P. & Perdok, W. G. (1955*b*). *Acta Cryst.* **8**, 521–524.

Hartman, P. & Perdok, W. G. (1955*c*). *Acta Cryst.* **8**, 525–529.

Hodsdon, J. H., Brown, G. M., Sieker, L. C. & Jensen, L. H. (1990). *Acta Cryst.* B**46**, 54–62.

Janin, J. & Rodier, F. (1995). *Proteins*, **23**, 580–587.

Jollès, P. & Berthou, J. (1972). *FEBS Lett.* **23**, 21–23.
Kabsch, W. & Sander, C. (1983). *Biopolymers*, **22**, 2577–1637.
Madhusudan, Kodandapani, R. & Vijayan, M. (1993). *Acta Cryst.* D**49**, 234–245.
Matsuura, Y. (1991). *J. Appl. Cryst.* **24**, 1063–1066.
Matsuura, Y., Hata, Y., Yamaguchi, T., Tanaka, N. & Kakudo, M. (1979). *J. Biochem.* **85**, 729–737.
Nadarajah, A. & Pusey, M. L. (1996). *Acta Cryst.* D**52**, 983–996.
North, A. C. T. & Phillips, D. C. (1968). *Acta Cryst.* A**24**, 351–359.
Rao, S. T. & Sundaralingam, M. (1996). *Acta Cryst.* D**52**, 170–175.
Rashkovich, L. N., Gvozdev, N. V. & Yaminsky, I. V. (1998). *Crystallography Report.* In the press.
Reid, R. C., Prausnitz, J. M. & Sherwood, T. K. (1985). *The Properties of Gases and Liquids.* New York: McGraw–Hill.
Singh, J. & Thornton, J. M. (1992). *Atlas of Protein Side-Chain Interactions*, Vol. 1. Oxford: IRL Press.
Steinrauf, L. K. (1959). *Acta Cryst.* **12**, 77–79.
Strom, C. S. & Bennema, P. (1997*a*). *J. Cryst. Growth*, **173**, 150–158.
Strom, C. S. & Bennema, P. (1997*b*). *J. Cryst. Growth*, **173**, 159–166.
Svensson, L. A., Dill, J., Sjölin, L., Wlodawer, A., Toner, M., Bacon, D., Moult, J., Veerapandian, B. & Gilliland, G. L. (1991). *J. Cryst. Growth*, **110**, 119–130.
Vaney, M. C., Maignan, S., Riès-Kautt, M. & Ducruix, A. (1996). *Acta Cryst.* D**52**, 505–517.